In situ investigation of D-glucose oxidation into value-added products on Au, Pt and Pd under alkaline conditions: a comparative study

Théo Faverge, Bruno Gilles, Antoine Bonnefont, Frédéric Maillard, Christophe Coutanceau, Marian Chatenet

In situ investigation of *D*-glucose oxidation into value-added products on Au, Pt and Pd under alkaline conditions: a comparative study

Théo Faverge,[†,‡] Bruno Gilles,[¶] Antoine Bonnefont,[‡,§] Frédéric Maillard,[‡,§] Christophe Coutanceau,[*,†,§] and Marian Chatenet[*,‡,§]

†*Université de Poitiers, IC2MP, UMR CNRS 7285, 4 Rue Michel Brunet, 86073 Poitiers Cedex 9, France*

‡*Univ. Grenoble Alpes, Univ. Savoie Mont Blanc, CNRS, Grenoble INP, LEPMI, 38000 Grenoble, France*

¶*Univ. Grenoble Alpes, Univ. Savoie Mont Blanc, CNRS, Grenoble INP, SIMAP, 38000 Grenoble, France*

§*French Research Network on Hydrogen (FRH2), Research federation n°2044 CNRS, France*

E-mail: christophe.coutanceau@univ-poitiers.fr; marian.chatenet@grenoble-inp.fr

Abstract

The mechanisms of oxidation of glucose, gluconic acid and sorbitol have been studied on gold, platinum and palladium using cyclic voltammetry (CV), differential electrochemical mass spectrometry (DEMS) and *in situ* Fourier Transform infrared spectroscopy (FTIRs). The nature of the reactant has a strong impact on the onset of the oxidation reaction. The anomeric function of glucose is oxidized at low potentials on the three surfaces, while gluconic acid and sorbitol poison the surface at low potentials. In addition, the nature of the metal surface leads to different reaction pathways. It is

proposed that the oxidation of glucose initiates *via* the partial dissociative adsorption of glucose into glucose adsorbates and H_{ad} for the three metal surfaces. These adsorbates are partially combined into H_2 on Au and oxidized into water on Pt and Pd. In addition, Au features the best activity, selectivity and specificity for glucose oxidation into gluconate at low potentials. The study points out a reactant, catalyst and potential dependent mechanism.

Keywords

Glucose oxidation, Non-enzymatic catalysis, Gluconic acid, Sorbitol, Gold, Platinum, Palladium, Reaction intermediates

Introduction

Fine chemistry historically relied on the fossil fuel industry, and especially on oil extraction and refining.[1] Progressive rarefaction of the resource combined to the adverse environmental consequences of its extraction are the main motivations to search for alternative sources of chemicals. One possible way to synthesize low carbon footprint chemicals is the use of non-edible biomass waste as a substitute.[2] In that context, cellulose extracted from biomass can play an important role, as it is a clean and widely accessible carbon source. *D*-glucose units constituting the cellulose can be further extracted from it and can lead to numerous chemicals of interest[3] such as sorbitol or gluconic acid (gluconate in alkaline media), respectively by selective reduction or oxidation, as presented in Fig. 1.

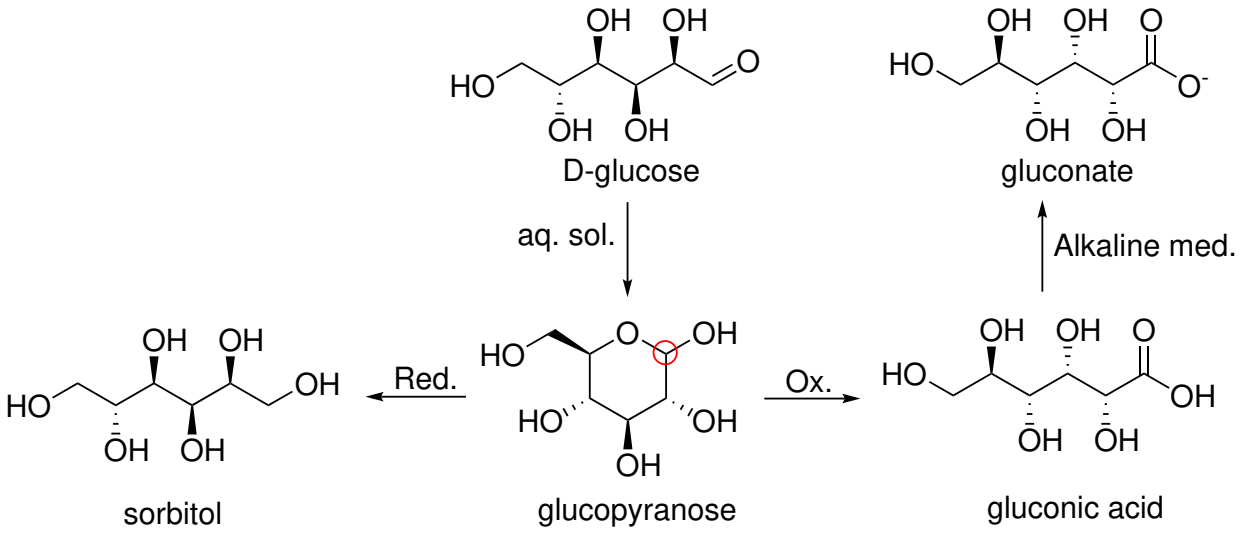

Fig. 1: The simple (electro)chemical reactions of glucose into value-added compounds. In aqueous solution, glucose is mainly under its cyclic form: glucopyranose, that presents an anomeric carbon (circled in red).

Glucose oxidation has been extensively studied to produce sensors for blood glucose monitoring in diabetes, mainly based on enzymatic oxidation.[4–6] Its use as a fuel for enzymatic fuel cells has equally been investigated for energy production[7] and powering of implantable devices.[8] Consequently, one major industrial way to produce gluconic acid from glucose oxidation is through the use of biotechnological processes.[9,10] Despite their high selectivity, these processes feature a number of disadvantages such as slow reaction rate, and complex separation and purification processes. The use of non-enzymatic catalysts to perform selective oxidation of glucose into gluconic acid (and the same for its selective reduction into sorbitol) could enable going beyond these limitations and could lead to an easy-to-control and continuous process. Brouzgou *et al.*[11] have reviewed the performance of non-enzymatic catalysts for glucose electrooxidation in direct glucose fuel cells and the mechanism proposed. This could be applied to paired-electrolyzers,[12] as schematized in Fig. 2. This setup allows to obtain at the same time and in separate compartments both products of interests, by coupling the anodic (glucose oxidation into gluconate) and cathodic (glucose reduction into sorbitol) reactions. The selective production of value-added compounds at

both electrodes of the system may help to decrease the overall electrical energy cost. In that system, appropriate separation between the anolyte and catholyte will be provided by using a dense ion-conductive membrane, likely an anion-exchange membrane. For such system, alkaline media are preferred to acidic ones because higher activities are achieved in the former electrolytes.[13]

In such media, Au-, Pd- and Pt-based catalysts display high activity. For example, Yan *et al.*[14] and Rafaïdeen *et al.*[15] evidenced the high activity of Pd_xAu_y/C catalysts towards glucose oxidation, the Pd_3Au_7 formulation being the most efficient. Neha *et al.* developed a very active and selective Pt_9Bi_1/C catalyst.[16] Because those noble metals are very interesting for the glucose oxidation reaction, the comparison of their individual electrocatalytic behavior is of paramount importance. Indeed, despite the great difference observed in shape and activity on the voltammograms, similar mechanisms are generally proposed for glucose oxidation on gold, platinum and palladium.

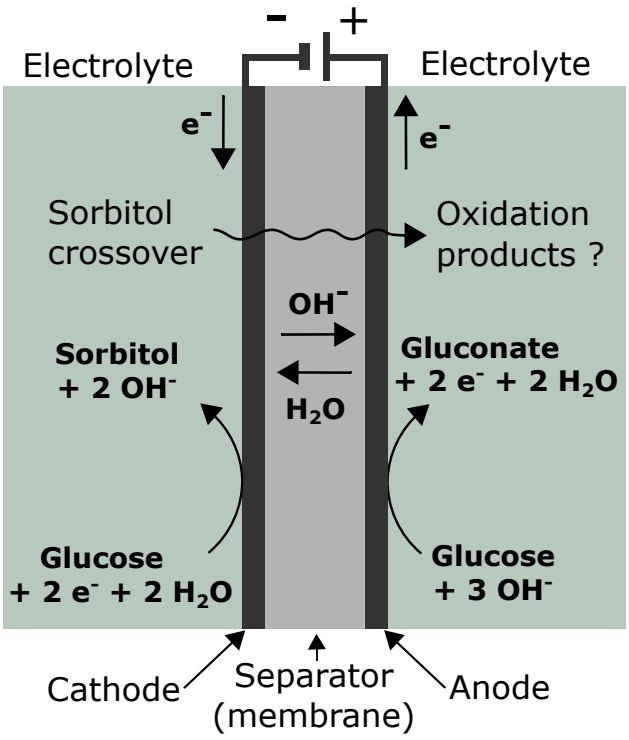

Fig. 2: Outline of a glucose paired-electrolysis cell.

Achieving a continuous process with good selectivity and specificity requires to investi-

gate the stability of the products obtained from glucose towards oxidation. At the positive electrode, electrooxidation of D-glucose to produce gluconic acid on various catalysts has been widely discussed.[17–22] Some authors investigated the effect of surface orientation on the catalyst activity for glucose oxidation.[23–25] It appeared that (100) surface domains were the most active ones for Au and Pd, whereas Pt (111) surface domains led to higher activity towards glucose oxidation. In comparison, few studies were carried out on gluconic acid oxidation.[26,27] Furthermore, as crossover of sorbitol (produced at the negative electrode) through the membrane cannot be excluded, its oxidation in the anode conditions has to be investigated equally.[28,29]

Herein, by combining Cyclic Voltammetry (CV), Differential Electrochemical Mass Spectrometry (DEMS) and Fourier Transform InfraRed (FTIR) spectroscopy, it is aimed to identify the reaction products formed from the oxidation of glucose, gluconic acid and sorbitol on polycrystalline (pc) gold, platinum and palladium in alkaline media. This latter information may serve to define the optimal operating conditions for an anion-exchange membrane glucose electrolyzer producing gluconate at the anode and sorbitol at the cathode. Indeed, based on the identification of intermediates/products by coupled techniques, catalyst and potential dependent mechanisms for glucose, gluconic acid and sorbitol oxidation on noble surfaces are discussed. Further, this discussion allows proposing the most active noble metal towards glucose oxidation and selective towards gluconic acid, over the more specific glucose oxidation potential range.

Experimental

For brevity, only the main procedures are described hereafter; supplementary data and detailed procedures are reported in supporting information.

Materials

D-(+)-glucose ($\geq$ 99.5 % purity), *D*-gluconic acid sodium salt and *D*-sorbitol (BioUltra, HPLC), both $\geq$ 99 % purity, were purchased from Sigma Aldrich; sodium hydroxide solution (50 % w/w) from Alfa Aesar; ethanol (96 % vol) from VWR chemicals; acetone ($\geq$ 99.8 % purity, analytical reagent grade) from Fisher chemicals and polycrystalline diamond paste DE-SY of 6, 3 and 1 µm from Presi. Ultrapure water (resistivity $>$ 18.2 MΩ.cm, $<$ 3 ppb Total Organic Carbon) was used to prepare all electrolytes, while argon (5.0 purity) was used to deaerate them. All chemicals were used as received, without further purification. Sputtering targets (4N purity) were purchased from Lesker (Pt) and Neyco (Au and Pd). FTIR electrodes (3N5 purity) were purchased from Mateck.

Electrochemical setup

Electrochemical measurements are performed at room temperature with a BioLogic SP-300 potentiostat, in a 4-electrode gas-tight glass cell. A rotating disk electrode (RDE) with a 0.0314 cm^2 tip of bulk polycrystalline metal is used as working electrode (WE). The counter electrode (CE) is a 2 cm^2 plate of glassy carbon (GC)[30,31] held by a gold wire. The reference electrode is a commercial reversible hydrogen electrode (RHE) coupled through a capacitive bridge (2 capacitors of 22 µF in series) to a platinum wire ended by a ca. ⌀2 mm sphere, used as a filter for high frequency noise.[32]

All glassware is cleaned in Caro's acid and then thoroughly rinsed with ultrapure water before use. Prior each experiment, the RDE tip is softly mirror polished with 1 µm diamond paste as abrasive, then subsenquently rinsed with acetone, ethanol and water while sonicated in ultrasonic bath. Finally, the tip is dried at around 100°C under air in a laboratory oven.

Electrochemical measurements are performed in 10^{-1} M NaOH + x M reducer with x = 0, 10^{-3} and 10^{-1} by successive addition of a concentrated solution in the cell. During the measurements, the RDE does not rotate to limit mass transport towards the working electrode and hence surface poisoning,[33] and a gentle flow of argon is maintained above the

electrolyte surface. Detailed experimental conditions and data obtained at 10^{-3} M are given in supporting information (Fig. SI-2, to SI-4).

Mass spectrometry setup

Cyclic voltammetry coupled to mass spectrometry is performed using a VMP2Z potentiostat in a dedicated spectroelectrochemical cell. This cell is physically separated from the mass spectrometer (QME 220 model from Pfeiffer Vacuum) by a porous steel frit, supporting 3 layers of porous hydrophobic PTFE membrane (Cobetter filtration, 20 µm thickness, 20 nm pore diameter) to ensure water tightness. A ca. 50 nm thick metal film deposited by sputtering on the top PTFE layer plays the role of WE. The counter electrode is a 2 cm^2 platinum grid. A RHE is used as reference, again associated with a platinum sphere through a capacitor bridge for noise reduction. The investigated concentrations are 10^{-2} M, 10^{-1} M and 1 M, prepared by successive addition of the appropriate reactant in supporting electrolyte.

Deposition of the thin films has been performed at room temperature with the magnetron sputtering technique using a pulsed DC power supply. The argon pressure during sputtering was 0.66 Pa and the power was 10 W with a DC voltage of 350 V. Atomic Force Microscopy revealed a compact arrangement of small grains (5-10 nm) with a small ($\sim$ 1-2 nm) RMS roughness. Using the same experimental conditions, similar films were deposited on flat silicon wafers for measurement of deposit thickness. It is known indeed that the morphology of sputtered films at room temperature is not dependent on the nature of the substrate.[34] The thickness of those layers was accurately deduced from X-ray Reflectivity measurements and led to the determination of the deposition rate (in $nm\,min^{-1}$) for each metal, which is then used to deposit layers with controlled thickness on PTFE substrate.

Gaseous or volatile species produced at the surface of the sputtered layer during CV are sucked through the PTFE and steel frit by a vacuum cascade, and then directed to the mass spectrometer. The acquisition of the representative ionic currents is made sequentially,

one specie at a time. The time allowed to each specie is then chosen to ensure its accurate detection, without over delaying the detection of the others (according to the sweep rate of CV). The sequence used is given in Table 1.

Table 1: DEMS measuring sequence settings.

Position	Target	m/z	Detection time (ms)
1	H_2	2	100
2	CO	28	100
3	HCO	29	100
4	H_2CO	30	100
5	O_2	32	100
6	CO_2	44	100
7	Ar	40	50
8	E (V *vs.* RHE)	-	10
9	Total pressure (mbar)	-	10

As expected, raw results show that no signal comes out from the baseline in the case of HCO and H_2CO fragments. Moreover, the simultaneity of the CO and CO_2 signals in any experiment suggests that CO is produced in the spectrometer as a fragment of CO_2, and not as a direct reaction product (Fig. SI-14). Thus, its signal is not considered as relevant for the determination of the reaction mechanism. Finally, the Ar signal is only used (as the measure of total pressure) to control that the experimental conditions remain as stationary as possible. For the sake of clarity, only the H_2 and CO_2 signals will be presented and discussed hereafter, after baseline correction.

In situ FTIR setup

The electrochemical setup for *in situ* Fourier transform infrared spectroscopy is similar to the DEMS setup described previously, with a CaF_2 prism beveled at 60° constituting the bottom of the electrochemical cell. A 0.785 cm^2 flat disk of the desired bulk polycrystalline metal used as WE was pressed on the top surface of the prism. This way, a thin film of

electrolyte (10^{-2} M of reducer in supporting electrolyte) is formed between the WE and the prism. Then, a series of chronoamperometric measurements is performed every 0.1 V from lower to higher potentials by a Metrohm Autolab PGSTAT302N potentiostat, and a FTIR spectrum is measured at each potential step.

The FTIR spectrometer is a Bruker Vertex 70V. After mounting the cell, the optic chamber is evacuated until 1.1 hPa by a vacuum pump to ensure that no atmospheric gas (especially H_2O and CO_2) disturbs the measurement. *Via* its liquid nitrogen cooled HgCdTe (MCT) detector, the spectrometer measures spectra from 730 cm^{-1} to 8000 cm^{-1}. The single-beam spectra were obtained by coadding 256 interferograms acquired at a 4 cm^{-1} spectral resolution with an interferometer frequency of 40 kHz and then Fourier transformed.

Transmission FTIR setup

FTIR measurements of reference electrolytes with controlled reducer concentrations ranging between 10^{-3} M and 1 M were performed using a liquid transmission cell, assembled with parallel CaF_2 windows (2 mm thick) separated by a 6 µm thick Mylar spacer. The spectrometer diaphragm was set to 0.5 mm to prevent detector saturation. All other optical parameters are kept identical to those described in the previous section. Unlike for previous FTIR measurements, the central compartment was continuously flushed with argon, due to insufficient tightness of the transmission cell under vacuum condition. With this setup, interference fringes due to multiple reflections between the inner faces of CaF_2 windows may appear.[35,36] As the wavelength spacing between two minima or maxima ($\Delta\nu$) is directly related to the pathlength d through $d = 1/2\Delta\nu$,[35] a tiny change in cell mounting leads to significant changes in the fringing pattern superimposed to the signal. Even if data post-processing allows suppressing these interferences[37] one simple and practical solution consists of slightly tilting the cell support, around 1°. This leads to a clear improvement in spectrum quality, and proper removal of the interferences.

Results

Cyclic voltammetry

Cyclic voltammetry has been performed on bulk polycrystalline gold, platinum and palladium electrodes to assess their electrocatalytic activity toward glucose, gluconic acid and sorbitol oxidation. Under those potential and pH conditions, previous study [38] proved that dissolution of the catalysts occurs at various rates, leading to an ECSA variation over the cycles. Thus, the ECSA normalized current are given only in supporting information, Fig. SI-1. Here, any potential region where glucose is oxidized but neither gluconic acid nor sorbitol is of great interest to perform specific and selective oxidation of glucose into gluconate. Cyclic voltammograms obtained on gold are reported in Fig. 3.

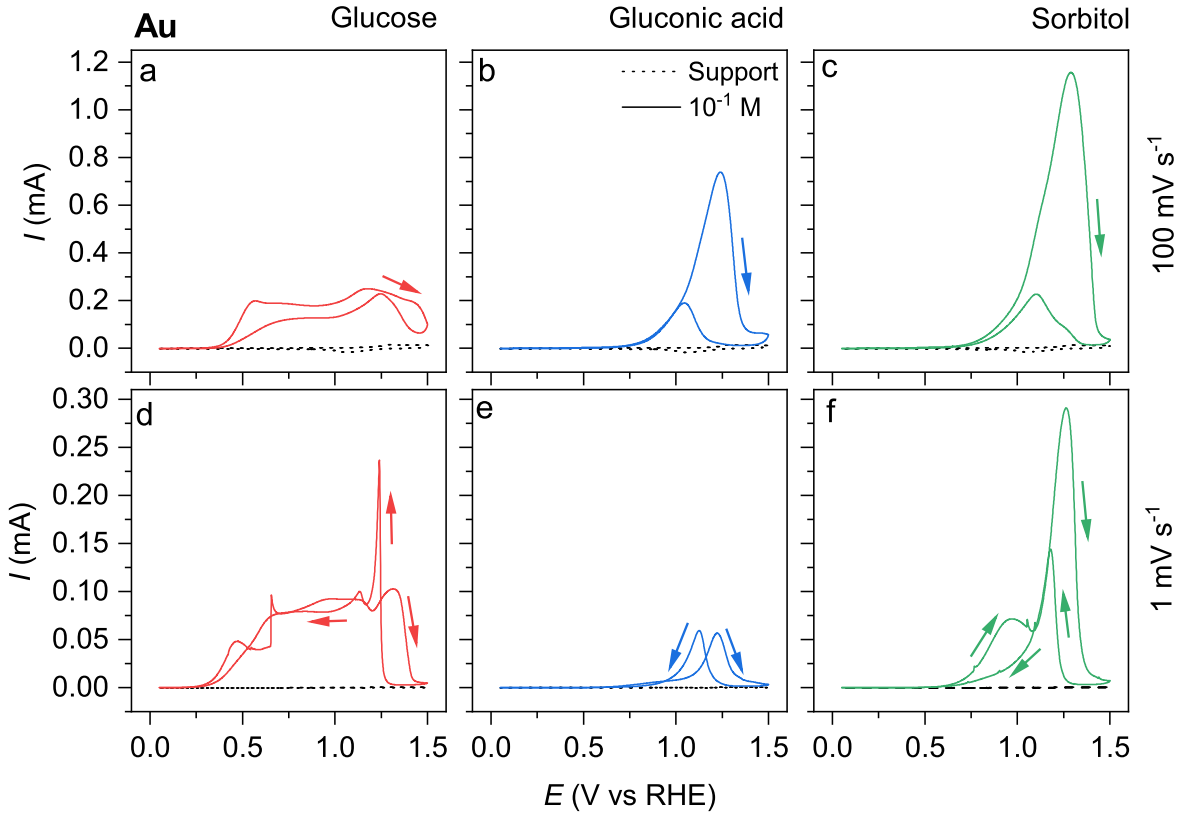

Fig. 3: Cyclic voltammograms of bulk Au in 10^{-1} M NaOH aqueous solution in the absence (black dotted line) or presence (coloured line) of 10^{-1} M reducer, at 100 (a, b, c) and 1 (d, e, f) mV s^{-1}, at room temperature. The ECSA was estimated to be ca. 5.42 x 10^{-2} cm^2.

Whatever the reactant, no significant current is measured below 0.25 V *vs.* RHE. In quasi-stationary conditions (i.e. at 1 $\mathrm{mV\,s^{-1}}$), the onset potential (measured at $I_{\mathrm{anodic}} =$ 3 µA, a current that significantly exceeds the baseline current in supporting electrolyte) is estimated to be around 0.29 V *vs.* RHE for glucose oxidation, and around 0.64 and 0.77 V *vs.* RHE for sorbitol and gluconic acid oxidation, respectively. The latter two reactants also produce similar cyclic voltammogram shapes, sorbitol leading to higher current densities than gluconic acid. Due to the formation of surface gold oxides,[39] a dramatic decrease of the oxidation current is observed at potentials exceeding 1.3 V *vs.* RHE. The reduction of the gold oxides during the cathodic scan frees the surface again (reactivation), allowing for further electrocatalysis, especially at low sweep rate (1 $\mathrm{mV\,s^{-1}}$) and for glucose, in agreement with the literature.[21,40] It leads to an oxidation peak (despite it was obtained during the negative scan) that likely depends on the combination of sweep rate, rate of gold oxide reduction and surface coverage with adsorbates formed at high potentials.

According to the onset potential values, the region between 0.30 and 0.65 V *vs.* RHE seems of great interest to oxidize specifically glucose on gold. To determine whether or not gluconate is effectively produced in that potential range, DEMS and FTIR have been used, and the results will be described later in this manuscript.

Similar measurements performed on a platinum electrode are reported in Fig. 4.

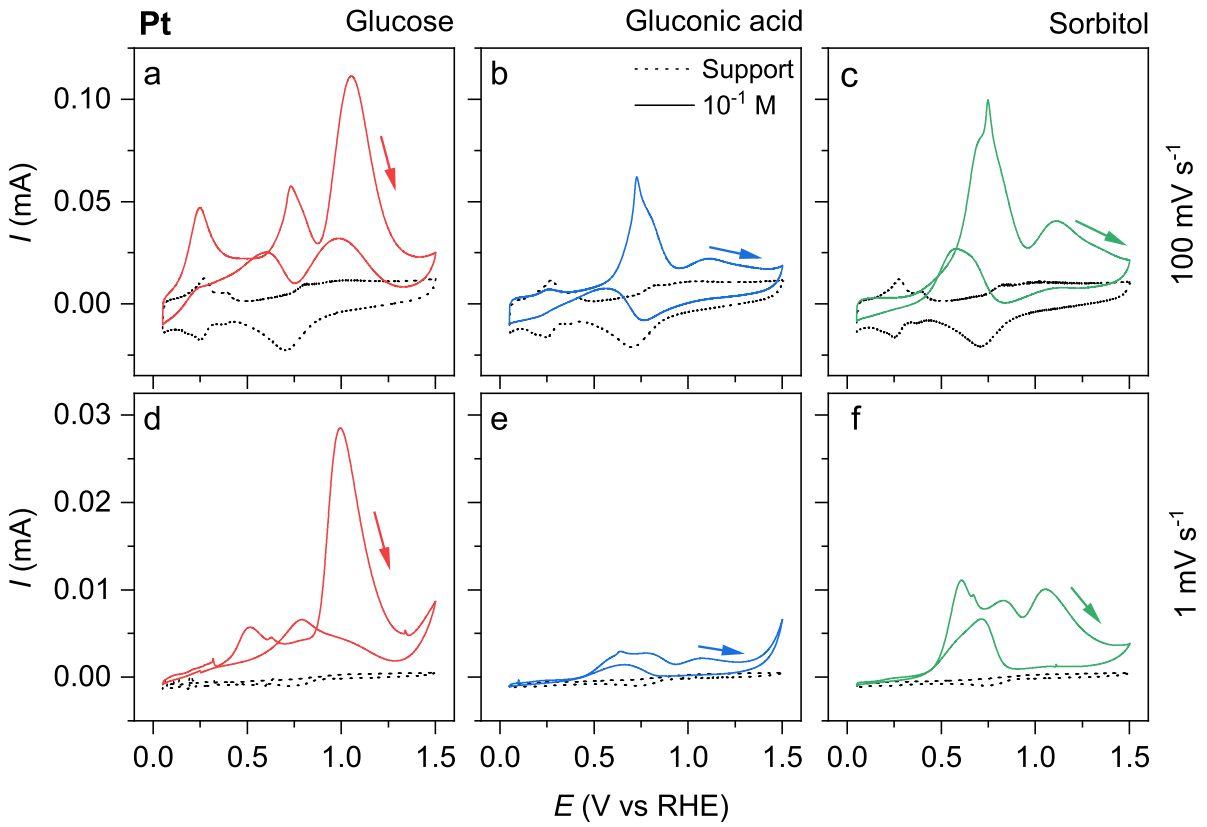

Fig. 4: Cyclic voltammograms of bulk Pt in 10^{-1} M NaOH aqueous solution in the absence (black dotted line) or presence (coloured line) of 10^{-1} M reducer, at 100 (a, b, c) and 1 (d, e, f) mV s^{-1}, at room temperature. The ECSA was estimated to be ca. 7.43 x 10^{-2} cm^2.

Compared to gold, glucose, gluconic acid and sorbitol oxidation on platinum starts at significantly lower potential, but the currents recorded are approximately 10 times lower. Moreover, the adsorption/desorption of underpotentially deposited hydrogen atoms (H_{UPD}) is inhibited at 100 mV s^{-1} during gluconic acid and sorbitol oxidation, suggesting surface poisoning. During glucose oxidation, an additional oxidation wave is observed in that region, particularly visible at 100 mV s^{-1}. This transient current is attributed to the oxidation of the adsorbates (glucose adsorbates and H_{UPD}) originating from glucose adsorption at low potentials. This point will be discussed in detail hereafter. Conversely to what was found on gold, no clear potential range where the glucose oxidation would be specific could be identified on platinum. But again, it is worth to note the similarity of the onset potential for the oxidation of gluconic acid and sorbitol and that of the shape of the corresponding voltammograms,

sorbitol still leading to higher current densities. Investigation of the products obtained by coupled techniques will determine if selective electrolysis of glucose is possible on Pt.

Finally, similar experiments on palladium are displayed in Fig. 5.

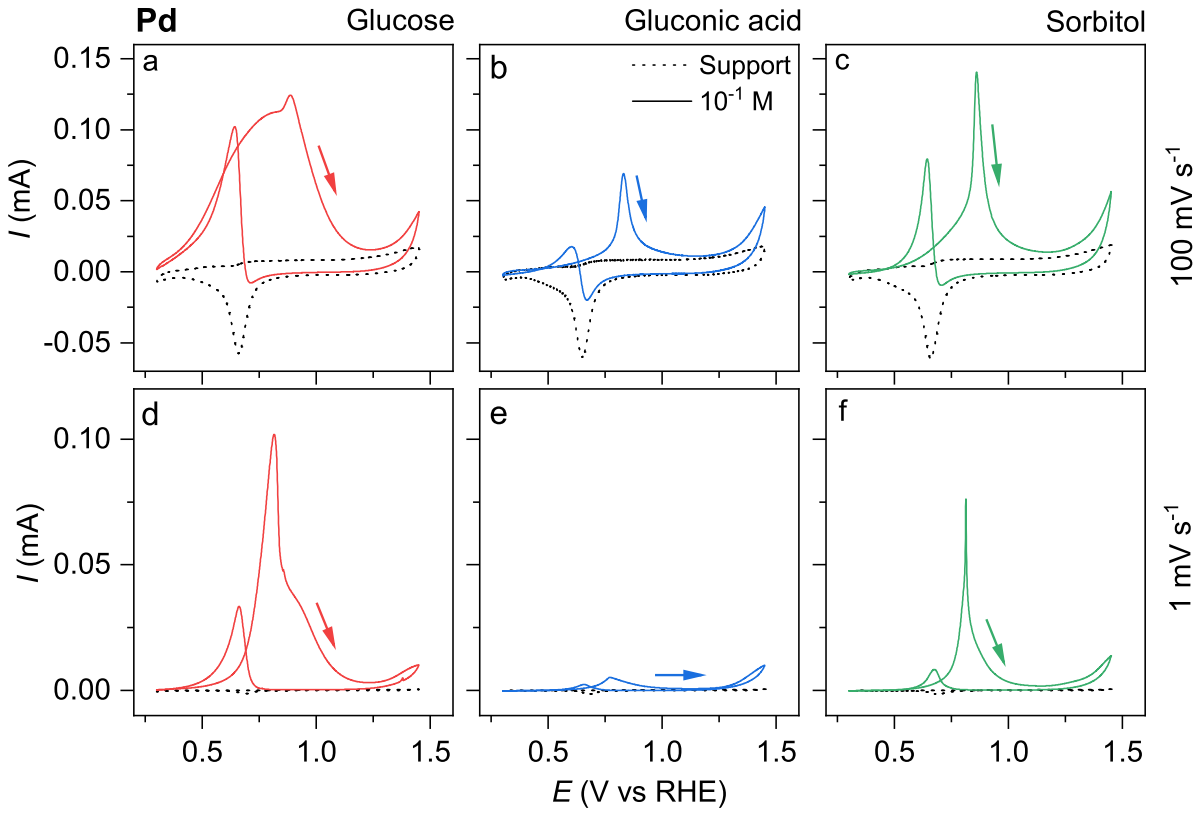

Fig. 5: Cyclic voltammograms of bulk Pd in 10^{-1} M NaOH aqueous solution in the absence (black dotted line) or presence (coloured line) of 10^{-1} M reducer, at 100 (a, b, c) and 1 (d, e, f) mV s^{-1}, at room temperature. The ECSA was estimated to be ca. 1.36 x 10^{-1} cm^2.

Similar to what was observed on Au and Pt, the reactivation of the Pd surface coincides with the reduction of surface oxides (particularly visible at 100 mV s^{-1}). Beyond this similarity during the negative scan, the behavior of Pd towards the oxidation of reactants is markedly different from those of Au and Pt. Indeed, for the positive potential scan, all oxidation steps are merged into one main peak centered around 0.7 - 0.8 V *vs.* RHE,[19] with glucose leading to a first oxidation wave starting from 0.4 V *vs.* RHE, particularly visible at 100 mV s^{-1}. A second oxidation peak, similar for every reactant, starts at potentials above 1.25 V *vs.* RHE.

Interestingly, Pd features nearly no activity for gluconic acid oxidation below 1.25 V *vs.* RHE. Charge calculation from 0.3 to 1.2 V *vs.* RHE has been performed at 1 $\mathrm{mV\,s^{-1}}$. It leads to 17.3 mC for glucose oxidation, while it is only 1.1 mC for gluconic acid, i.e. more than 15 times lower.

From this series of voltammograms, one can conclude that all metal surfaces are electrocatalytically active towards glucose, sorbitol and gluconic acid oxidation but deactivate at high potentials, as a result of metal-oxide formation. Thus, during the negative scan, every catalyst reactivates as a result of surface oxide reduction. As the onset potential and the CV shapes are similar for gluconic acid and sorbitol on all surfaces, and sorbitol has only alcohol groups, it is reasonable to propose that the same kind of chemical groups are adsorbed/oxidized in both these molecules, i.e. alcohol groups. The difference in current densities recorded, especially clear on Pd, may come from higher poisoning of the surface by $\mathrm{CHOH-COO^-}$ groups, or hindering of the surface by adsorbed species.

Regarding the onset potential of oxidation, gold appears to be more specific towards glucose than towards gluconic acid or sorbitol oxidation at low potentials, while palladium appears to be non-specific. Based on this criterion, Au appears to be the best candidate to specifically oxidize glucose, and Pd the worst. *In situ* characterization of the reaction products remains mandatory to confirm if the potential operating zones identified allow to reach a satisfactory selectivity towards gluconate.

Differential Electrochemical Mass Spectrometry

To shed fundamental light into the mechanisms of glucose, gluconic acid or sorbitol oxidation, Differential Electrochemical Mass Spectrometry measurements have been performed using porous sputtered metallic thin films as working electrodes. Fig. 6 displays the electrochemical current and the ionic current for $m/z = 2$ (H_2) and $m/z = 44$ (CO_2) as a function of the electrode potential. At equilibrium in alkaline media, no CO_2 should be

present in solution, as its stable form is carbonates.[41] In the DEMS configuration, as any gaseous specie produced at the sputtered layer is directly sucked by the vacuum cascade, CO_2 is directed to the detector before having a chance to form carbonates in the solution. Another possible explanation that cannot be excluded here would be a local pH shift, as it is the case for FTIR measurements (Fig. SI-17). In this case, carbonates could be produced at lower potential without being detected by the mass spectrometer. Raw results showing the temporal evolution of potential, H_2 and CO_2 signal in parallel are given Fig. SI-5 to SI-13. The measurements performed in supporting electrolyte and in the presence of reducer at 10^{-2} M are shown in black dotted / colour solid lines, respectively.

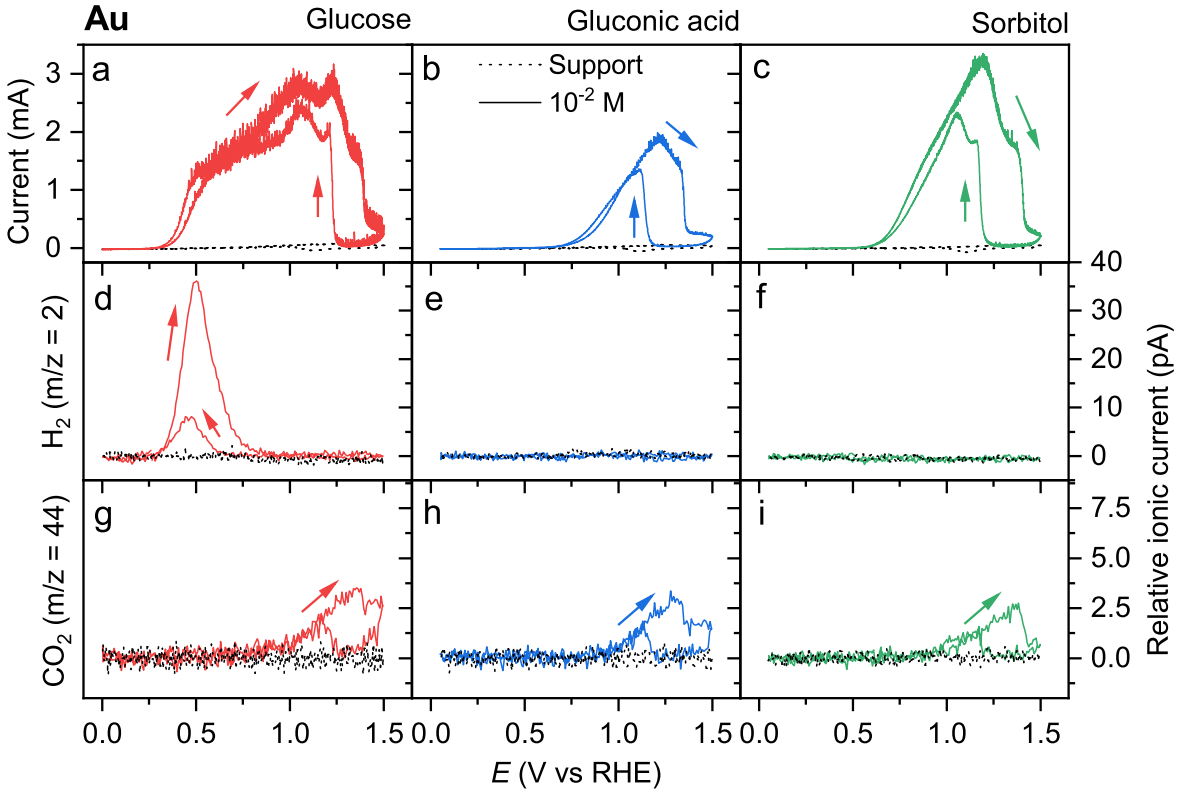

Fig. 6: DEMS signal obtained by CV on a Au sputtered thin layer in 10^{-1} M NaOH aqueous solution in the absence (black dotted line) or presence (coloured line) of 10^{-2} M reducer, at 10 mV s^{-1} and at room temperature. The electrochemical current is reported in panels a, b, c, while relative ionic current of H_2 and CO_2 are reported in panels d, e, f and g, h, i, respectively.

The cyclic voltammograms measured on a gold sputtered thin film agree with the results obtained on a bulk RDE (Fig. 3). Hence, it can reasonably be assumed that the electrochemical processes investigated here are at least similar to those described in the previous section, despite slightly different operating conditions (notably in terms of working electrode geometry and cell configuration).

The $m/z = 44$ signal is similar for each reducer, with CO_2 being produced mainly during the anodic scan above 1 V *vs.* RHE, and in a smaller amount during the cathodic scan immediately above 1 V *vs.* RHE. As CO_2 production reveals C-C bond breakage, 1 V *vs.* RHE seems to be the upper bound in these conditions to avoid uncontrolled oxidation of the 3 compounds studied here. As discussed in the previous section, the upper limit of specific glucose oxidation was anyway set around 0.65 V *vs.* RHE to avoid undesired further oxidation of the products. *In situ* FTIR will determine if gluconate is produced between 0.30 and 0.65 V *vs.* RHE under these conditions on gold.

No H_2 is detected during gluconic acid or sorbitol oxidation. In contrast, a strong H_2 signal is measured during glucose oxidation from 0.3 to 0.8 V *vs.* RHE, again stronger during the positive scan than during the negative scan. This signal corresponds to the first oxidation process described in the previous section, in a potential region where Au is inactive for gluconic acid and sorbitol oxidation. In a recent contribution, Neha *et al.*[42] proposed that this signal comes from the dissociative adsorption (partial dehydrogenation) of glucose on gold through its anomeric function, absent on gluconic acid and sorbitol. This process leads to the formation of metastable H_{ad} species.[39] At this potential, the electrooxidation of H_{ad} on gold surface is slow (Fig. SI-15). Thus, H_{ad} adsorbates are able to diffuse onto the metal surface, until they recombine (Tafel step) into molecular hydrogen and desorb, hence the $m/z = 2$ signal detection.[43]

The case of platinum is slightly different from gold, results are given in Fig. 7.

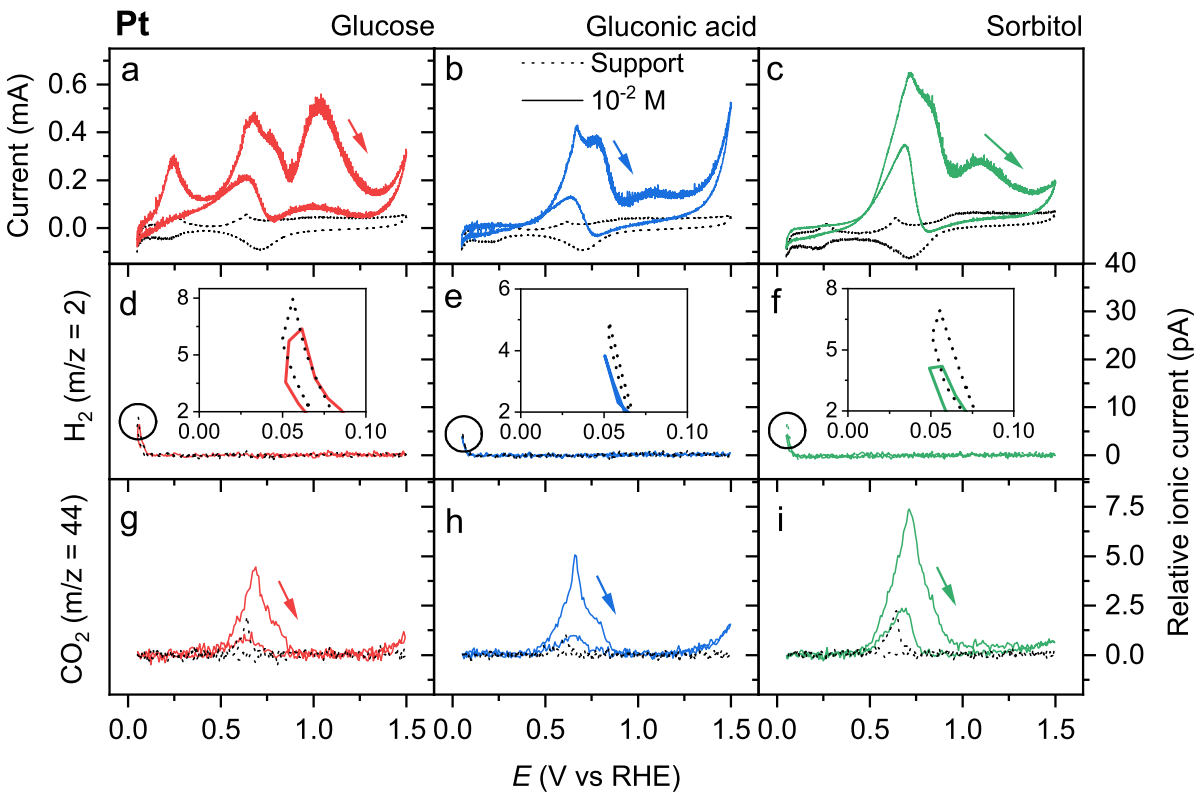

Fig. 7: DEMS signal obtained by CV on a Pt sputtered thin layer in 10^{-1} M NaOH aqueous solution in the absence (black dotted line) or presence (coloured line) of 10^{-2} M reducer, at 10 mV s^{-1} and at room temperature. The electrochemical current is reported in panels a, b, c, while relative ionic current of H_2 and CO_2 are reported in panels d, e, f and g, h, i, respectively. Insets are a zoomed view on the HER region.

Whatever the reducer, CO_2 is produced mainly in the range from 0.45 to 1.00 V *vs.* RHE on platinum, corresponding to the second glucose oxidation wave, shown in Fig. 4. This CO_2 production could be attributed to the oxidation of CO_{ad} species coming from dissociative adsorption of glucose on platinum at low potentials[44] by combination with surface OH_{ad} species formed in the 0.45 to 1.00 V *vs.* RHE range through a Langmuir-Hinshelwood pathway. Another possible explanation would be the oxidation of the adsorbates from each reactant in the region where the metal surface covers with OH_{ad} species. One also notes that Fig. 7 indicates an absence of CO_2 generation in the Pt-oxides regions (E > 1 V vs RHE), which suggest a different glucose oxidation mechanism on Pt and Pt-oxides. This will be further addressed in the discussion section. In any case, these features demonstrate that

Pt is neither specific nor selective for such glucose-like fuels, at potentials higher than 0.45 V *vs.* RHE.

Regarding H_2 production, the same behavior is observed for every reducer: H_2 is produced through hydrogen evolution reaction (HER) at low potentials (in supporting electrolyte, dotted line) and the addition of reactant leads to a small decrease of the hydrogen current measured in the same potential range (see inset graphs). This is attributed to a decreased number of available sites on the electrode surface for HER due to reducer molecules adsorption onto the surface. It can be proposed that the first step of glucose adsorption is similar on platinum and gold, leading to H_{ad} formation.[42] The difference is that on Pt at positive potentials, H_{ad} species are directly oxidized into protons and released in solution, before having a chance to recombine into molecular hydrogen. This should lead to a significant change in the local pH at the interface, and explains why no hydrogen signal ($m/z = 2$) is detected in the 0.1 - 0.4 V *vs.* RHE region, although there is a well-defined oxidation current, which must, therefore, at least partly originate from the oxidation of H_{ad} species resulting from the dissociative adsorption of glucose.

Finally, the result obtained on Pd are reported in Fig. 8.

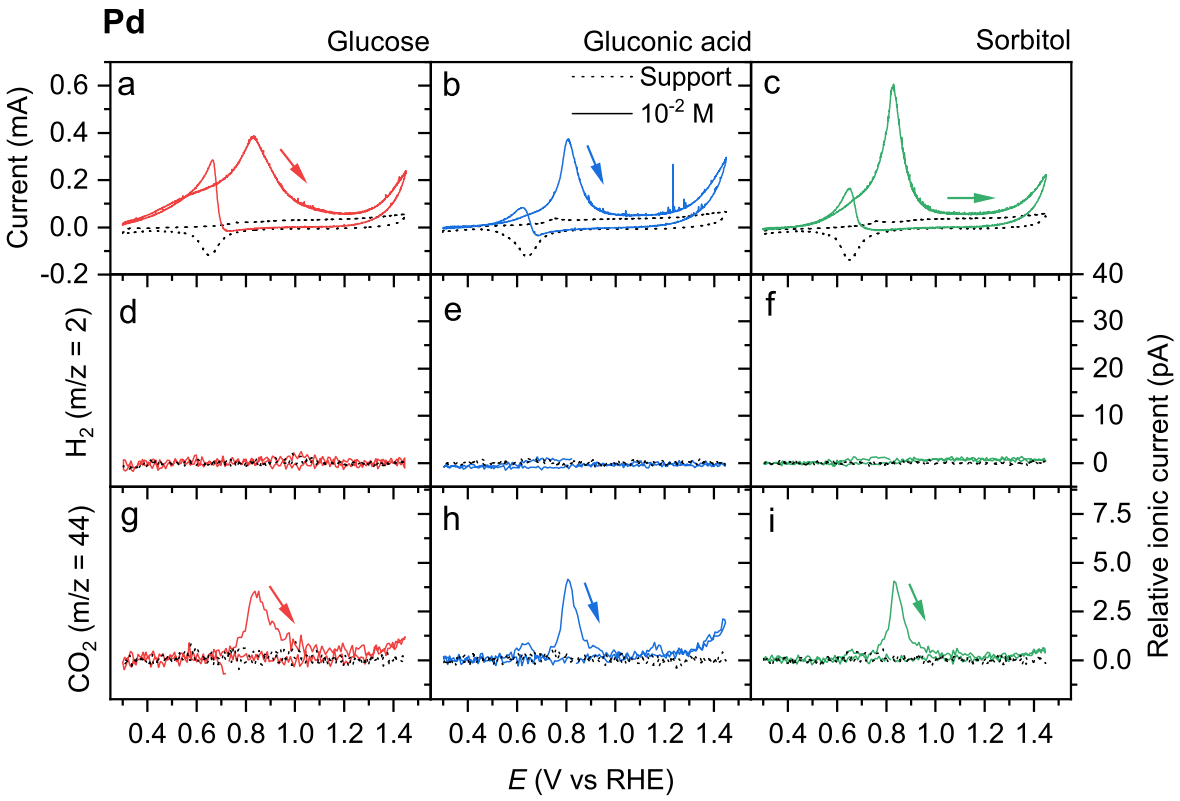

Fig. 8: DEMS signal obtained by CV on a Pd sputtered thin layer in 10^{-1} M NaOH aqueous solution in the absence (black dotted line) or presence (coloured line) of 10^{-2} M reducer, at 10 mV s^{-1} and at room temperature. The electrochemical current is reported in panels a, b, c, while relative ionic current of H_2 and CO_2 are reported in panels d, e, f and g, h, i, respectively.

Due to a common H_2 scale (chosen to allow a rapid comparison between Fig. 6, 7 & 8) it seems that no H_2 is detected on Pd. However, raw results provided in supporting information (Fig. SI-12 & SI-13) show that a small but significant baseline change is observed during gluconic acid and sorbitol oxidation. Low H_2 signal is measured at low potentials, and conversely, higher H_2 signal is measured at higher potentials. This can be explained by the formation of adsorbed H (H_{ad}) from dissociative adsorption of the fuels onto the Pd surface that can partly be inserted into the Pd structure as absorbed H (H_{ab}) below 0.3 V vs RHE.[45] Below 0.7 V *vs.* RHE the desorption of H_{ab} hydrides is impeded by the presence of the adsorbed organic species.[46] Above 0.7 V *vs.* RHE, Pd surface oxides can be formed and facilitates the oxidation of the adsorbed organic species, leading to the shoulder before

the main oxidation peak. A small part of the H_{ad} species recombine to form H_2,[47] but most of H_{ab} can go to the surface and be electrochemically oxidized to form water and leave free sites.

Concerning CO_2 production, Pd behaves mostly as Pt, with a main peak located from 0.7 to 1.0 V *vs.* RHE, followed by a smaller peak at high potential, regardless of the reducer. The main CO_2 production peak coincides with the main oxidation peak measured by cyclic voltammetry, and is delayed by around 200 mV compared to the Pt surface. This is attributed to the blockage of the surface by the H_{ab} and glucose-like species. Then above 0.7 V *vs.* RHE, free metallic sites are available to stabilize OH_{ad} species and oxidize organic adsorbates into CO_2.

It is worth noticing that the major difference between glucose and gluconic acid measured at 1 $mV\,s^{-1}$ by cyclic voltammetry on bulk electrodes (Fig. 5) nearly disappeared when using a Pd sputtered electrode. This can be attributed to the roughness difference, leading to a micro-reactor effect, to an increased residence time, or to a higher defects density. This questions the selectivity of palladium for glucose oxidation into gluconate, the blocking of the Pd electrode by organic adsorbates depending on the trade-off between the gluconic acid concentration and the active surface area.

DEMS measurements allowed to partially determine which species are produced during the oxidation of glucose, gluconic acid and sorbitol. Molecular H_2 is produced only on gold with glucose. It is proposed that glucose adsorption at low potentials leads to the formation of H_{ad} on every catalyst studied here. Then, these adsorbates are oxidized into protons onto Pt, partially recombine into H_2 on Au (Fig. SI-16) and form hydrides at low potentials on Pd. As this hydrogen production on gold is neither observed for gluconic acid nor sorbitol, it is proposed that glucose adsorbs through its anomeric function, absent in the other reactants. In any case, the adsorbates formed from gluconic acid and sorbitol seem much more stable than the ones from glucose, which deactivate any of the metal surfaces at low potential

values in the former cases. CO_2, which comes from C-C bond breakage and thus is to avoid, is detected on each catalyst, but at significantly higher potentials on gold than on the other catalysts: gold is therefore the most promising of these noble catalysts to perform selective oxidation of glucose at low potentials. Finally, the electrode roughness seems to have an important (and unequal between the reactants) effect on the activity, at least on Pd. Thus, comparison with the results obtained on bulk material has to be done carefully.

Transmission FTIR

For the identification of numerous products which are not gaseous and so cannot be detected by DEMS, *in situ* FTIR is a valuable technique. The spectra obtained in transmission for each compound at 1 M in 10^{-1} M NaOH are given in Fig. 9. Due to insufficient signal over noise ratio, the transmission spectra obtained at lower concentrations did not allow to evidence characteristic bands. Thus, they are not presented for brevity. Compared to the baseline at a transmittance value of 1, a downward peak reveals higher absorption of the corresponding wavenumber, and thus the presence of an additional bond. Conversely, an upward peak reveals the consumption of the corresponding species.

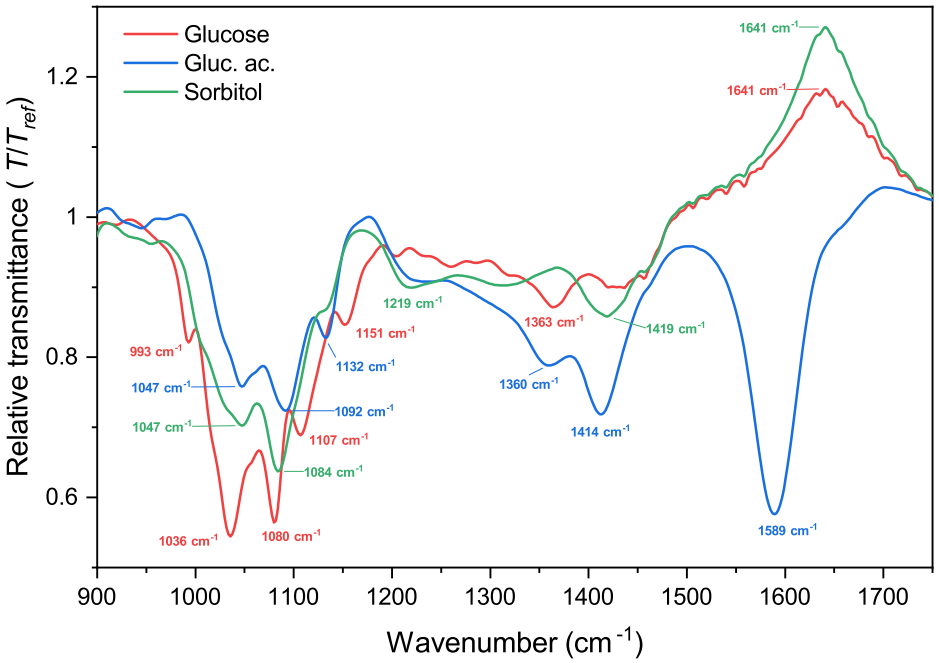

Fig. 9: Transmission spectra of 1 M reactant in supporting electrolyte.

The wavenumber region comprised from 1000 to 1200 cm^{-1} exhibits numerous bands, assigned to the different vibration modes of alcohol groups.[48] These groups are present in great number for each reactant, and are thus poorly specific. In addition, under *in situ* conditions, this range is cut by the CaF_2 prism, leading to a dramatic increase of the noise. This leads us to discard this range in the spectra's analysis. In contrast, the wavenumber region comprised between 1200 cm^{-1} and 1750 cm^{-1} allows identifying the specific bands of each reactant and their relative intensities (weak w, medium md, strong s, and very strong vs) as follows:

- Glucose: 1363 cm^{-1} (w)
- Gluconic acid: 1360 cm^{-1} (md), 1414 cm^{-1} (s) and 1589 cm^{-1} (vs)
- Sorbitol: 1219 cm^{-1} (w) and 1419 cm^{-1} (w)

The positive band at 1641 cm^{-1} observed with glucose and sorbitol is attributed to bending vibrational mode of water[49] ($\nu_2 = 1654$ cm^{-1}). As the electrolyte has to be changed between experiments, this effect can be due to a lower amount of electrolyte (and so water) between

the cell windows during measurement at 1 M compared to the reference measurement in supporting electrolyte. Moreover, the main bands characteristics of gluconic acid will be sought in the next section as evidence of its production.

In situ FTIR

In situ FTIR spectra have been measured during the oxidation of each reactant on bulk electrodes, revealing the production of intermediates through the apparition of various negative bands in the region from 1200 to 1750 cm^{-1}. The main ones are assigned in Table 2.

Table 2: FTIR band indexation.

Index	Wavenumber	Vibration	Proposed species	Ref
a	1309 cm^{-1}	ν_{sym} O=C-O	HCO_3^-	50–52
b	1352 cm^{-1}	ν_{CO} or δ_{CH_2}	gluconolactone / gluconate	16,17
c	1385 cm^{-1}	ν_{sym} O=C-O	CO_3^{2-}	50–52
d	1411 cm^{-1}	ν_{sym} O=C-O	gluconate	16,17
e	1582 cm^{-1}	ν_{asym} O=C-O	gluconate	16,17

The band a and c are respectively ascribed to the formation of bicarbonate and carbonate ions, coming from CO_2 dissolution in alkaline media (Fig. SI-17). These bands evidence C-C bond breakage from uncontrolled oxidation, which is undesirable. Conversely, the combination of the bands b, d and e is attributed to the formation of gluconate, in agreement with the reference spectra displayed in Fig. 9. The pseudo-band f at ca. 1720 - 1725 cm^{-1}, visible on the spectra recorded on Au and also sometimes visible on spectra recorded on Pt and Pd surfaces, cannot be definitely attributed. It either can be due to the baseline change at wavenumbers higher than 1750 cm^{-1}, or to the formation of gluconic acid because of pH decrease at the electrode/electrolyte interface. Indeed, the comparison of gluconic acid and gluconate spectra available in the spectral database for organic compounds[53] indicates that the band at 1735 cm^{-1} for gluconic acid is missing for gluconates.

The spectra obtained during oxidation of glucose, gluconic acid and sorbitol on polycrystalline gold, platinum and palladium leads to Fig. 10. Spectra are given with larger scale in supporting information, Fig. SI-18 to SI-20.

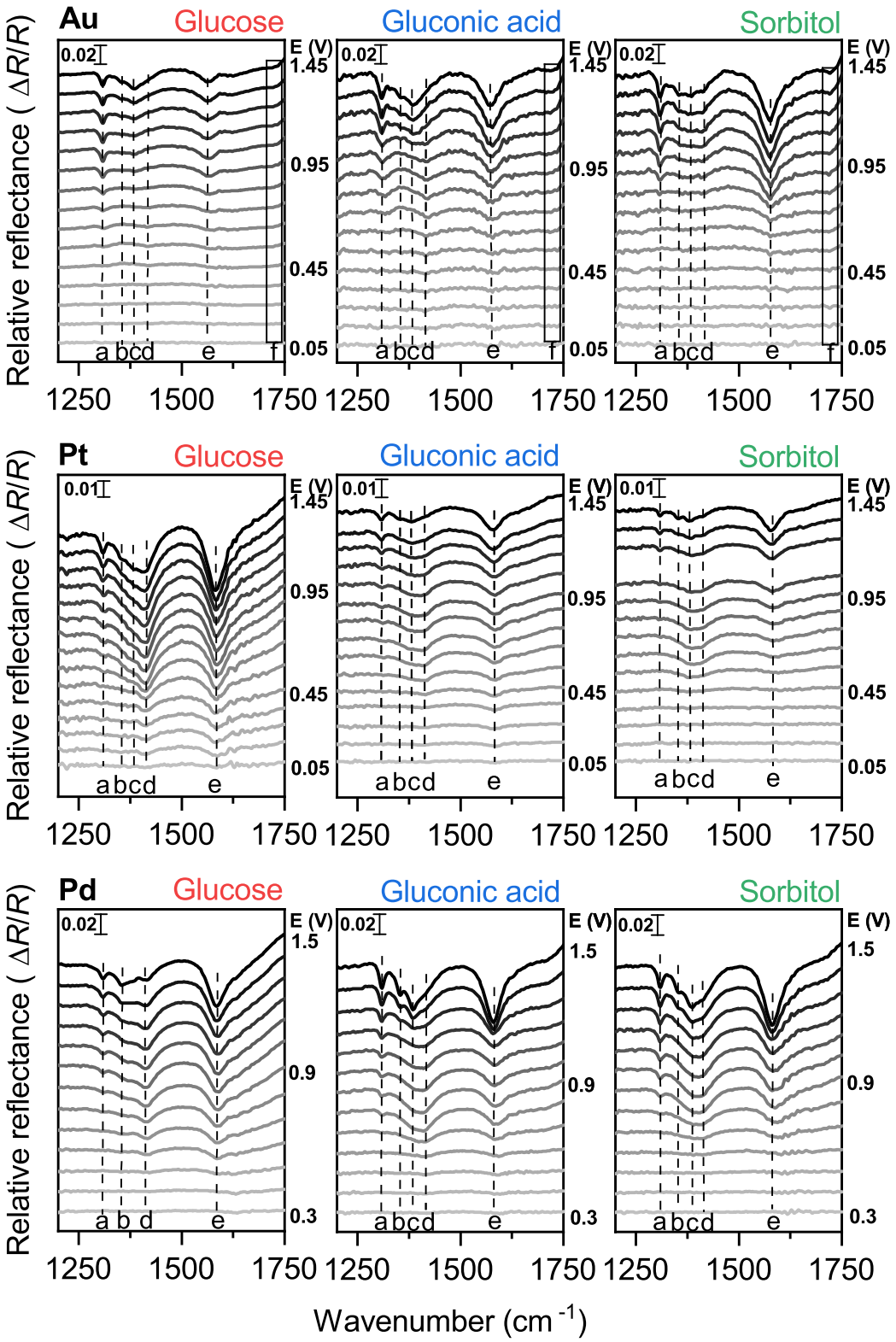

Fig. 10: FTIR spectra obtained on bulk Au (upper panels), Pt (middle panels) and Pd (lower panels). Reactant concentration is 10^{-2} M in 10^{-1} M NaOH. The Relative reflectance scale bar is twice smaller for Pt, owing to the smaller currents of reducer's oxidation on that metal versus Au and Pd.

FTIR allowed to evidence glucose oxidation on gold starting from 0.45 V *vs.* RHE, which is consistent with the onset potential value measured by cyclic voltammetry. The bands from gluconate (d and e) are slightly visible in the 0.45 - 0.85 V *vs.* RHE region. The hydrogenocarbonate band is growing concomitantly to the bands d and e, while the band c, attributed to the formation of carbonates, appears only at 0.95 V *vs.* RHE, in agreement with the value measured in Fig. 6. This can be rationalized by considering the prevalence diagram of carbonate species,[41] a strong pH shift occurred in the electrolyte thin film due to OH^- consumption before 0.95 V *vs.* RHE. This evidences that oxidation of glucose into gluconate occurs with correct specificity on gold in the potential range from 0.45 to 0.85 V *vs.* RHE.

Gluconic acid oxidation FTIR spectra evidenced that the bands d and e also appear but at higher potentials, around 0.65 V *vs.* RHE. This value is slightly lower than what was obtained by cyclic voltammetry (0.75 V *vs.* RHE). In the case of sorbitol, the band e appears first, at 0.75 V *vs.* RHE. In order to avoid further oxidation of the gluconate produced, selective oxidation of glucose should then be performed in the 0.45 - 0.65 V *vs.* RHE region on gold. At higher potentials, DEMS and FTIR results evidenced that uncontrolled oxidation occurs, producing CO_2, carbonates, and possibly other short chain molecules.

As expected from the cyclic voltammetry experiment, platinum is highly active for glucose oxidation. Indeed, the band d and e attributed to gluconate are clearly visible already at 0.15 V *vs.* RHE. However, the bands c from carbonates appear at 0.45 V *vs.* RHE, which is consistent with the DEMS results, Fig. 7. This leads to a very narrow potential window in which it is possible to oxidize selectively glucose on Pt. In addition, FTIR spectra obtained during gluconic acid oxidation evidence that the reaction initiates at ca. 0.15 V *vs.* RHE (band e). In real conditions, gluconic acid produced from glucose would likely get further oxidized at any potential, evidencing that Pt is a very non-selective catalyst.

Palladium appears to be active for glucose oxidation from 0.5 V *vs*, but produces CO_2 above 0.7 V *vs.* RHE, leading also to a narrow operating range. Moreover, Pd is equally

active for gluconic acid and sorbitol oxidation, also from 0.5 V *vs.* RHE. Gluconate produced from glucose oxidation would be further oxidized, as well as on Pt, leading to a complete loss of the selectivity, hence further demonstrating that Pd cannot be considered a selective catalyst for glucose oxidation into gluconate.

Discussion

Although *in situ* infrared measurements reveal that the oxidation of all reducers produces carboxylates whatever the surfaces studied here, cyclic voltammetry and DEMS measurements point towards very different mechanisms of oxidation from one reducer to the other and from one surface to the other. The first step of glucose electrooxidation on noble metal surfaces generally proposed consists of the adsorption of the anomeric function through dehydrogenation forming Metal-Glucose (noted M-Glu hereafter, with M = Au, Pt or Pd) adsorbate according to the following reaction:[17,18]

$$C_6H_{12}O_6 + 2\,M \longrightarrow M{-}C_6H_{11}O_6 + M{-}H \tag{1}$$

On Au surface, H_2 is produced from the onset potential of glucose oxidation at ca. 0.35 V to ca. 0.8 V *vs.* RHE, whereas no CO_2 is detected by DEMS over this potential range. FTIRS measurements indicate that the main reaction product over this potential range is gluconate. Therefore, it is proposed that the first voltammetric wave corresponds to the following reactions:

$$2\,Au{-}H \longrightarrow 2\,Au + H_2 \tag{2}$$

$$Au{-}Glu + 2\,OH^- \longrightarrow Au + \text{gluconate}\,(C_6H_{11}O_7^-) + H_2O + 1\,e^- \tag{3}$$

The recombination of H_{ad} (noted Au-H) on Au surface to produce H_2 (Eq. 2) was already observed in the case of borohydride electrooxidation on gold electrode,[54] and discussed

elsewhere.[55,56] However, the adsorption of OH^- at gold surfaces (Eq. 3) has been shown to start from ca. 0.4 V *vs.* RHE on Au surface,[57] therefore it is likely that the following reactions can take place from this potential:

$$Au + OH^- \longrightarrow Au{-}OH + 1\,e^- \tag{4}$$

$$Au{-}H + Au{-}OH \longrightarrow 2\,Au + H_2O \tag{5}$$

$$Au{-}Glu + Au{-}OH + OH^- \longrightarrow Au + \text{gluconate } (C_6H_{11}O_7^-) + H_2O \tag{6}$$

Reactions 2 and 3 are likely predominant from 0.35 V to 0.5 V *vs.* RHE on mainly metallic Au surface,[24] whereas reactions 4 to 6 become predominant from 0.5 V *vs.* RHE, explaining the peak of H_2 production whereas no current decay was observed on the corresponding CV.

For potentials higher than 0.8 V *vs.* RHE, corresponding to the second electrochemical feature in CVs, DEMS measurements show no hydrogen production, indicating that reaction 2 does no more occur, totally replaced by reactions 4 and 5. In the same potential range, CO_2 formation is detected. Accordingly, FTIRS measurements detect the formation of carbonate from 0.95 V *vs.* RHE, but also the footprint absorption bands of gluconate. It is then proposed that, in this potential range, mainly gluconate and some overoxidized (glucaric acid[20]) and degradation products (from C5 to C1, including CO_2/carbonate) are formed[58] (in particular in the thin-electrolyte layer configuration of the FTIRS experiments).

On Pt surface, DEMS measurements did not show any production of hydrogen from glucose adsorption over the whole studied potential range. FTIRS measurements indicate that gluconate started to be formed from very low potentials, close to 0.1 V *vs.* RHE. CO_2 is only detected between ca. 0.5 V and 0.9 V *vs.* RHE by DEMS measurements. It is then proposed that during the first voltammetric feature between 0.05 V and 0.4 V *vs.* RHE, corresponding to the hydrogen region of Pt, the following reactions occur:

$$Pt{-}H + OH^- \longrightarrow Pt + H_2O + 1\,e^- \tag{7}$$

$$\mathrm{Pt{-}Glu} + 2\,\mathrm{OH^-} \longrightarrow \mathrm{Pt} + \text{gluconate}\ (\mathrm{C_6H_{11}O_7^-}) + \mathrm{H_2O} + 1\,\mathrm{e^-} \tag{8}$$

But the decrease of the current from 0.1 V *vs.* RHE seems to indicate that the surface starts to be partly blocked by adsorbed species, such as carbon monoxide ($\mathrm{CO_{ad}}$) and/or gluconolactone ($\mathrm{Gluco_{ad}}$).[17,42]

In the second voltammetric feature between 0.4 V and 0.9 V *vs.* RHE, $\mathrm{CO_2}$ is detected by DEMS measurements. FTIRS measurements confirmed this result by displaying the absorption band of carbonate from 0.45 V *vs.* RHE. These observations indicate that gluconate, overoxidized and degradation products are formed. The following reactions are then proposed in this potential range:

$$\mathrm{Pt} + \mathrm{OH^-} \longrightarrow \mathrm{Pt{-}OH} + 1\,\mathrm{e^-} \tag{9}$$

$$\mathrm{Pt} + \text{glucose} + \mathrm{OH^-} \longrightarrow \mathrm{Pt{-}Glu} + \mathrm{H_2O} + 1\,\mathrm{e^-} \tag{10}$$

$$\mathrm{Pt} + \text{glucose} + 2\,\mathrm{OH^-} \longrightarrow \mathrm{Pt{-}Gluco} + 2\,\mathrm{H_2O} + 2\,\mathrm{e^-} \tag{10'}$$

$$\mathrm{Pt} + \text{glucose} + \mathrm{x\ OH^-} \longrightarrow \mathrm{Pt{-}CO} + \text{overoxidized/degradation products} \tag{10"}$$

$$\mathrm{Pt{-}Glu} + \mathrm{Pt{-}OH} + \mathrm{OH^-} \longrightarrow \mathrm{Pt} + \text{gluconate}\ (\mathrm{C_6H_{11}O_7^-}) + \mathrm{H_2O} \tag{11}$$

$$\mathrm{Pt{-}Gluco} + \mathrm{OH^-} \longrightarrow \mathrm{Pt} + \text{gluconate}\ (\mathrm{C_6H_{11}O_7^-}) + \mathrm{H_2O} \tag{12}$$

$$\mathrm{Pt{-}Gluco} + \mathrm{y\ OH^-} \longrightarrow \mathrm{Pt{-}CO} + \text{overoxidized/degradation products} \tag{13}$$

$$\mathrm{Pt{-}CO} + \mathrm{Pt{-}OH} + \mathrm{OH^-} \longrightarrow 2\,\mathrm{Pt} + \mathrm{CO_2} + \mathrm{H_2O} + 1\,\mathrm{e^-} \tag{14}$$

The feature at higher potentials, between 0.85 V and 1.25 V *vs.* RHE corresponds to complex reactions occurring at the oxidized surface of platinum. According to FTIRS measurements, gluconate seems to be still the main formed product. But overoxidized and/or degradation products could also be formed at so high electrode potentials. The reactions do

not involve glucose adsorption with CO and CO_2 formation, but C-C bond breaking forming C4 to C2 products could occur. However, DEMS measurements indicate also that oxidation of gluconic acid leads to CO_2 production only between ca. 0.5 V and 1.0 V *vs.* RHE. This could indicate that overoxidized compounds, such as glucaric acid and ketogluconic acids,[58] are formed at higher potentials.

Except for the supplementary sharp oxidation peaks centered at ca. 0.9 V *vs.* RHE at high scan rate and ca. 0.8 V *vs.* RHE at low scan rate (Fig. 5), the behavior of the Pd surfaces towards glucose oxidation in the middle potentials region (from 0.5 V to 1.0 V *vs.* RHE), where CO_2 was detected by DEMS, is similar to that of Pt surfaces and same processes as in the case of Pt can be proposed over this potential range. It is proposed that the superimposed sharp peak comes from the de-insertion of H_{ab} to H_{ad} and to the oxidation of H_{ad} into water at the Pd surface. Indeed, in the potential region of the first step of glucose adsorption ($E < 0.3$ V *vs.* RHE), Pd is able to insert H_{ad} into his structure.[45]

Conclusion

This study identified major difference in activity and selectivity for the oxidation of glucose into gluconate between gold, platinum and palladium. Despite their high activity for the reaction, Pt and Pd show poor selectivity for gluconate production. Indeed, DEMS and FTIR evidenced C-C bond breakage through the production of CO_2, carbonates and bicarbonates at potentials close to the onset potential for the reaction. Worse, FTIR demonstrates that the oxidation of gluconic acid or sorbitol occurs at the same potential as the oxidation of glucose on these two metals. It leads to a negligible selectivity, as any gluconate molecule produced by glucose oxidation will immediately be oxidized again. The first oxidation wave measured by cyclic voltammetry for glucose oxidation and absent for gluconic acid or sorbitol oxidation is then partially attributed to the oxidation H_{ad} species formed onto the surface by dissociative adsorption of the glucose molecule through its anomeric function.

Conversely, the production of CO_2 and carbonates is delayed to ca. 0.95 V *vs.* RHE on gold, while the reaction onset for glucose oxidation is around 0.3 V *vs.* RHE, and around 0.7 V *vs.* RHE for gluconic acid and sorbitol oxidation. Thus, the potential range from 0.3 to ca. 0.7 V *vs.* RHE is of great interest to perform selective oxidation of glucose into gluconate on gold. In addition, DEMS measurements evidenced H_2 as a byproduct in this potential range, which is easy to separate and valorise.

Finally, one must underline a pronounced need to perform long-term electrolysis of a glucose solution on a gold electrode maintained in the conditions described above. The analysis of the products present in the electrolyte after electrolysis by high performance liquid chromatography (HPLC) or assimilated techniques would then provide relevant results on the catalyst selectivity.

Supporting Information Available

The Supporting Information is available free of charge on the ACS Publications website. Experimental conditions detailed, additional experimental results from mass spectrometry and FTIR spectroscopy.

Acknowledgement

This study was funded by the french national research agency (ANR): grant ANR-20-CE43-0005. TF and MC thank Vincent Martin for his help in the DEMS measurements and Thierry Encinas for the X-ray characterisation of the sputtered thin films.

References

(1) Levi, P. G.; Cullen, J. M. Mapping global flows of chemicals: from fossil fuel feedstocks to chemical products. *Environmental Science and Technology* **2018**, *52*, 1725–1734.

(2) Saygin, D.; Gielen, D. J.; Draeck, M.; Worrell, E.; Patel, M. K. Assessment of the technical and economic potentials of biomass use for the production of steam, chemicals and polymers. *Renewable and Sustainable Energy Reviews* **2014**, *40*, 1153–1167.

(3) Song, J.; Fan, H.; Ma, J.; Han, B. Conversion of glucose and cellulose into value-added products in water and ionic liquids. *Green Chemistry* **2013**, *15*, 2619–2635.

(4) Reach, G.; Wilson, G. S. Can continuous glucose monitoring be used for the treatment of diabetes. *Analytical Chemistry* **1992**, *64*, 381A–386A.

(5) Wang, J. Electrochemical glucose biosensors. *Chemical Reviews* **2008**, *108*, 814–825.

(6) Heller, A.; Feldman, B. Electrochemistry in diabetes management. *Accounts of Chemical Research* **2010**, *43*, 963–973.

(7) Xu, S.; Minteer, S. D. Enzymatic biofuel cell for oxidation of glucose to CO2. *ACS Catalysis* **2012**, *2*, 91–94.

(8) Cosnier, S.; Le Goff, A.; Holzinger, M. Towards glucose biofuel cells implanted in human body for powering artificial organs: Review. *Electrochemistry Communications* **2014**, *38*, 19–23.

(9) Hustede, H.; Haberstroh, H.-J.; Schinzig, E. Gluconic acid. *Ullmann's Encyclopedia of Industrial Chemistry* **2000**, *17*, 39–44.

(10) Anastassiadis, S.; Morgunov, I. Gluconic acid production. *Recent Patents on Biotechnology* **2007**, *1*, 167–180.

(11) Brouzgou, A.; Tsiakaras, P. Electrocatalysts for Glucose Electrooxidation Reaction: A Review. *Topics in Catalysis* **2015**, *58*, 1311–1327.

(12) Cao, Y.; Knijff, J.; Delparish, A.; D'Angelo, M. F. N.; Noel, T. A Divergent Paired Electrochemical Process for the Conversion of Furfural Using a Divided-Cell Flow Microreactor. *ChemSusChem* **2021**, *14*, 590–594.

(13) Lamy, C.; Coutanceau, C.; Baranton, S. In *Production of clean hydrogen by electrochemical reforming of oxygenated organic compounds*; Pollet, B., Ed.; Hydrogen and Fuel cells primers, Elsevier: Amsterdam, 2020.

(14) Yan, L.; Brouzgou, A.; Meng, Y.; Xiao, M.; Tsiakaras, P.; Song, S. Efficient and poison-tolerant PdxAuy/C binary electrocatalysts for glucose electrooxidation in alkaline medium. *Applied Catalysis B: Environmental* **2014**, *150-151*, 268–274.

(15) Rafaïdeen, T.; Baranton, S.; Coutanceau, C. Highly efficient and selective electrooxidation of glucose and xylose in alkaline medium at carbon supported alloyed PdAu nanocatalysts. *Applied Catalysis B: Environmental* **2019**, *243*, 641–656.

(16) Neha, N.; Kouamé, B. R. S.; Rafaïdeen, T.; Baranton, S.; Coutanceau, C. remarkably efficient carbon-supported nanostructured platinum-bismuth catalysts for the selective electrooxidation of glucose and methyl-glucoside. *Electrocatalysis* **2021**, *12*, 1–14.

(17) Beden, B.; Largeaud, F.; Kokoh, K. B.; Lamy, C. Fourier transform infrared reflectance spectroscopic investigation of the electrocatalytic oxidation of D-glucose: Identification of reactive intermediates and reaction products. *Electrochimica Acta* **1996**, *41*, 701–709.

(18) Pasta, M.; La Mantia, F.; Cui, Y. Mechanism of glucose electrochemical oxidation on gold surface. *Electrochimica Acta* **2010**, *55*, 5561–5568.

(19) Becerik, I.; Kadirgan, F. The electrocatalytic properties of palladium electrodes for the oxidation of d-glucose in alkaline medium. *Electrochimica Acta* **1992**, *37*, 2651–2657.

(20) Schlegel, N.; Wiberg, G. K.; Arenz, M. On the electrooxidation of glucose on gold: Towards an electrochemical glucaric acid production as value-added chemical. *Electrochimica Acta* **2022**, *410*, 140023.

(21) Moggia, G.; Kenis, T.; Daems, N.; Breugelmans, T. Electrochemical oxidation of d-

glucose in alkaline medium: impact of oxidation potential and chemical side reactions on the selectivity to d-gluconic and d-glucaric acid. *ChemElectroChem* **2020**, *7*, 86–95.

(22) Haynes, T.; Dubois, V.; Hermans, S. Particle size effect in glucose oxidation with Pd/CB catalysts. *Applied Catalysis A: General* **2017**, *542*, 47–54.

(23) Popović, K. D.; Marković, N. M.; Tripković, A. V.; Adžić, R. R. Structural effects in electrocatalysis. Oxidation of D-glucose on single crystal platinum electrodes in alkaline solution. *Journal of Electroanalytical Chemistry* **1991**, *313*, 181–199.

(24) Adzic, R. R.; Hsiao, M. W.; Yeager, E. B. Electrochemical oxidation of glucose on single crystal gold surfaces. *Journal of Electroanalytical Chemistry and Interfacial Electrochemistry* **1989**, *260*, 475–485.

(25) Rafaïdeen, T.; Baranton, S.; Coutanceau, C. Pd-shaped nanoparticles modified by gold ad-atoms: Effects on surface structure and activity toward glucose electrooxidation. *Frontiers in Chemistry* **2019**, *7*, 1–10.

(26) Besson, M.; Flèche, G.; Fuertes, P.; Gallezot, P.; Lahmer, F. Oxidation of glucose and gluconate on Pt, Pt Bi, and Pt Au catalysts. *Recueil des Travaux Chimiques des Pays-Bas* **1996**, *115*, 217–221.

(27) Dirkx, J. M.; van der Baan, H. S. The oxidation of gluconic acid with platinum on carbon as catalyst. *Journal of Catalysis* **1981**, *67*, 14–20.

(28) Dimitratos, N.; Porta, F.; Prati, L.; Villa, A. Synergetic effect of platinum or palladium on gold catalyst in the selective oxidation of D-sorbitol. *Catalysis Letters* **2005**, *99*, 181–185.

(29) Torres-Pacheco, L. J.; Osornio-Villa, A.; García-Gómez, N. A.; Olivas, A.; Valdez, R.; Guerra-Balcázar, M.; Álvarez-Contreras, L.; Arjona, N. Effect of AuM (M: Ag, Pt &

Pd) bimetallic nanoparticles on the sorbitol electro-oxidation in alkaline medium. *Fuel* **2020**, *274*, 117864.

(30) Chen, J. G.; Jones, C. W.; Linic, S.; Stamenkovic, V. R. Best practices in pursuit of topics in heterogeneous electrocatalysis. *ACS Catalysis* **2017**, *7*, 6392–6393.

(31) Chatenet, M.; Benziger, J.; Inaba, M.; Kjelstrup, S.; Zawodzinski, T.; Raccichini, R. Good practice guide for papers on fuel cells and electrolysis cells for the Journal of Power Sources. *Journal of Power Sources* **2020**, *451*, 227635.

(32) Herrmann, C. C.; Perrault, G. G.; Pilla, A. A. Dual reference electrode for electrochemical pulse studies. *Analytical Chemistry* **1968**, *40*, 1173–1174.

(33) Tominaga, M.; Nagashima, M.; Nishiyama, K.; Taniguchi, I. Surface poisoning during electrocatalytic monosaccharide oxidation reactions at gold electrodes in alkaline medium. *Electrochemistry Communications* **2007**, *9*, 1892–1898.

(34) Mahan, J. E. In *Physical Vapor Deposition of Thin Films*; John Wiley & Sons,, Ed.; Wiley-Interscience: New York, 2000; p 340.

(35) Hawranek, J. P.; Neelakantan, P.; Young, R. P.; Jones, R. N. The control of errors in i.r. spectrophotometry-III. Transmission measurements using thin cells. *Spectrochimica Acta Part A: Molecular Spectroscopy* **1976**, *32*, 85–98.

(36) Konevskikh, T.; Ponossov, A.; Blümel, R.; Lukacs, R.; Kohler, A. Fringes in FTIR spectroscopy revisited: Understanding and modelling fringes in infrared spectroscopy of thin films. *Analyst* **2015**, *140*, 3969–3980.

(37) Mayerhöfer, T. G.; Pahlow, S.; Hübner, U.; Popp, J. Removing interference-based effects from infrared spectra-interference fringes re-revisited. *Analyst* **2020**, *145*, 3385–3394.

(38) Schalenbach, M.; Kasian, O.; Ledendecker, M.; Speck, F. D.; Mingers, A. M.;

Mayrhofer, K. J.; Cherevko, S. The Electrochemical Dissolution of Noble Metals in Alkaline Media. *Electrocatalysis* **2018**, *9*, 153–161.

(39) Jaksic, M. M.; Johansen, B.; Tunold, R. Electrochemical behaviour of gold in acidic and alkaline solutions of heavy and regular water. *International Journal of Hydrogen Energy* **1993**, *18*, 91–110.

(40) A. Larew, L.; Johnson, D. C. Concentration dependence of the mechanism of glucose oxidation at gold electrodes in alkaline media. *Journal of Electroanalytical Chemistry* **1989**, *262*, 167–182.

(41) Zeebe, R. E.; Wolf-Gladrow, D. *CO2 in seawater : equilibrium, kinetics, isotopes*; Elsevier Oceanography Series: Amsterdam, 2001; p 346.

(42) Neha, N.; Rafaïdeen, T.; Faverge, T.; Maillard, F.; Chatenet, M.; Coutanceau, C. Revisited Mechanisms for Glucose Electrooxidation at Platinum and Gold Nanoparticles. *Electrocatalysis* **2022**, 121–130.

(43) Cornejo-Romero, J.; Solis-Garcia, A.; Vega-Diaz, S. M.; Fierro-Gonzalez, J. C. Reverse hydrogen spillover during ethanol dehydrogenation on TiO2-supported gold catalysts. *Molecular Catalysis* **2017**, *433*, 391–402.

(44) Bae, I. T.; Yeager, E.; Xing, X.; Liu, C. C. In situ infrared studies of glucose oxidation on platinum in an alkaline medium. *Journal of Electroanalytical Chemistry* **1991**, *309*, 131–145.

(45) Grdeń, M.; Łukaszewski, M.; Jerkiewicz, G.; Czerwiński, A. Electrochemical behaviour of palladium electrode: Oxidation, electrodissolution and ionic adsorption. 2008.

(46) Braesch, G.; Bonnefont, A.; Martin, V.; Savinova, E. R.; Chatenet, M. Borohydride oxidation reaction mechanisms and poisoning effects on Au, Pt and Pd bulk electrodes:

From model (low) to direct borohydride fuel cell operating (high) concentrations. *Electrochimica Acta* **2018**, *273*, 483–494.

(47) Gabrielli, C.; Grand, P. P.; Lasia, A.; Perrot, H. Investigation of hydrogen insertion in palladium using permeation transfer function techniques. *Journal of Electroanalytical Chemistry* **2002**, *532*, 121–131.

(48) Pouchert, C. J. *The Aldrich library of infrared spectra*, 3rd ed.; Aldrich Chemical Co.: Milwaukee, Wis., 1981; p 1203.

(49) Stomp, M.; Huisman, J.; Stal, L. J.; Matthijs, H. C. Colorful niches of phototrophic microorganisms shaped by vibrations of the water molecule. *The ISME Journal* **2007**, *1*, 271–282.

(50) Su, C.; Suarez, D. L. In Situ Infrared Speciation of Adsorbed Carbonate on Aluminum and Iron Oxides. *Clays and Clay Minerals 1997 45:6* **1997**, *45*, 814–825.

(51) Socrates, G. *Infrared and Raman characteristic group frequencies. Tables and charts*, 3rd ed.; John Wiley & Sons, Ltd: London, 2001; p 347.

(52) Lafforgue, C.; Maillard, F.; Martin, V.; Dubau, L.; Chatenet, M. Degradation of Carbon-Supported Platinum-Group-Metal Electrocatalysts in Alkaline Media Studied by in Situ Fourier Transform Infrared Spectroscopy and Identical-Location Transmission Electron Microscopy. *ACS Catalysis* **2019**, 5613–5622.

(53) AIST, Spectral Database for Organic Compounds SDBS, accessed on 2022-10-27. `https://sdbs.db.aist.go.jp/sdbs/cgi-bin/direct_frame_top.cgi`.

(54) Belén Molina Concha, M.; Chatenet, M.; Lima, F. H.; Ticianelli, E. A. In situ Fourier transform infrared spectroscopy and on-line differential electrochemical mass spectrometry study of the NH3BH3 oxidation reaction on gold electrodes. *Electrochimica Acta* **2013**, *89*, 607–615.

(55) Carabineiro, S. A.; Nieuwenhuys, B. E. Adsorption of small molecules on gold single crystal surfaces. *Gold Bulletin* **2009**, *42*, 288–301.

(56) Watkins, W. L.; Borensztein, Y. Mechanism of hydrogen adsorption on gold nanoparticles and charge transfer probed by anisotropic surface plasmon resonance. *Physical Chemistry Chemical Physics* **2017**, *19*, 27397–27405.

(57) Beden, B.; Çetin, I.; Kahyaoglu, A.; Takky, D.; Lamy, C. Electrocatalytic oxidation of saturated oxygenated compounds on gold electrodes. *Journal of Catalysis* **1987**, *104*, 37–46.

(58) Kokoh, K. B.; Léger, J. M.; Beden, B.; Huser, H.; Lamy, C. "On line" chromatographic analysis of the products resulting from the electrocatalytic oxidation of d-glucose on pure and adatoms modified Pt and Au electrodes—Part II. Alkaline medium. *Electrochimica Acta* **1992**, *37*, 1909–1918.

TOC Graphic